

Comparative performance of different energy storage devices in AGC of multi-source system including geothermal power plant

Washima Tasnin, and Lalit Chandra Saikia

Citation: [Journal of Renewable and Sustainable Energy](#) **10**, 024101 (2018); doi: 10.1063/1.5016596

View online: <https://doi.org/10.1063/1.5016596>

View Table of Contents: <http://aip.scitation.org/toc/rse/10/2>

Published by the [American Institute of Physics](#)

Comparative performance of different energy storage devices in AGC of multi-source system including geothermal power plant

Washima Tasnin^{a)} and Lalit Chandra Saikia^{b)}

Electrical Engineering Department, National Institute of Technology Silchar, Silchar, Assam, India

(Received 21 November 2017; accepted 27 February 2018; published online 16 March 2018)

This paper highlights an attempt of comparing the performance of several energy storage (ES) devices such as battery ES, flywheel ES, capacitive ES, superconducting magnetic ES, ultra-capacitors, and redox flow batteries (RFBs) in automatic generation control of an interconnected system. The considered system comprises conventional thermal, hydro, wind, and solar photovoltaic generations wherein a geothermal power plant (GTPP) is also incorporated. The thermal and hydro systems are provided with appropriate generation rate constraints. A new fractional order (FO) cascade controller named as the FO proportional-integral-FO proportional-integral-derivative (FOPI-FOPID) is proposed as a secondary controller, and its performance is compared with the commonly used classical controllers. A powerful stochastic algorithm called the Sine Cosine Algorithm has been used to optimize the controller gains and other parameters. Analyses of the dynamic responses reveal the superiority of FOPI-FOPID over the others in terms of settling time, peak deviation, and magnitude of oscillation. The effect due to introduction of GTPP has been examined, and the responses disclose that integration of GTPP leads to better dynamics. The comparison of performances of various ES devices in the presence of the FOPI-FOPID controller highlights the predominance of RFB over others. *Published by AIP Publishing.* <https://doi.org/10.1063/1.5016596>

I. INTRODUCTION

Electrical power systems comprise several utilities that are interconnected together to form large systems, which in spite of being complex are dynamic in nature. The exchange of power among these utilities is carried out over tie-lines. In order to attain proper interconnected operation of the power system, the frequency, voltage profile, and load flow configuration must be maintained at the scheduled level. This is achieved by controlling the real and reactive powers. Automatic generation control (AGC) plays a major role in maintaining the system frequency at nominal value and tie-line power flow at their scheduled values both in normal conditions and during small perturbations.¹⁻³ Some investigations on AGC⁴⁻⁶ reveal interesting facts, which have been done in the past few decades. Nanda *et al.*⁴ presented AGC of three unequal area thermal systems with an integral (I) controller. Saikia *et al.*⁵ studied various multi-area systems like two, three, and five areas, but their investigations were limited only to thermal systems. Sahu *et al.*⁶ studied AGC of two area thermal systems and further extended it up to multi-source power systems like thermal, hydro, and gas plants. All the above studies⁴⁻⁶ mainly focus on AGC for conventional generation, and no attention has been paid to the non-conventional (NC) energy sources. Due to rapid depletion of the conventional energy resources and harmful carbon emission issues, alternative NC sources came into picture to fulfil the future energy demands. Moreover, NC energy sources are preferred due to their abundancy. Solar and wind

^{a)}washima.nits@gmail.com

^{b)}lcsaikia@yahoo.com

energy are the most dominant ones, and their applications are prevalent in Ref. 7. Sharma and Saikia⁸ proposed the harnessing of solar energy by incorporating the solar thermal (ST) plant which uses parabolic trough. While integration of a dish Stirling solar thermal system with AGC is studied by Rahman *et al.*,⁹ Asano *et al.*¹⁰ developed the model of a solar photovoltaic system (SPV) for integrating it with AGC, but their study is limited to only rooftop generation. Lee and Wang¹¹ and Pan and Das¹² have studied the AGC for a distributed generation system where a microgrid with many generating sources is considered. Thus, SPV studies in AGC are restricted to stand-alone hybrid systems. Modelling of renewable energy (RE) sources like solar and wind is dealt in numerous literatures.⁷⁻¹² Thus, integration of renewable energy (RE) sources especially SPV may lead to several prospects of further research. Another RE source which is a potential candidate throughout the globe for medium and large scale generation of electricity and space heating is the geothermal energy (GE). GE belongs to the category of thermal energy which the earth stores inside itself automatically and thus is derived from the earth crust directly.¹³ Setel *et al.*¹⁴ discuss the prospects of using GE for electricity production at average temperatures. Although GE is a distinct source for harnessing electricity, the same is not yet included in AGC studies. Thus, geothermal power plants (GTPPs), along with the earlier existing renewable sources like wind and solar, can add a new dimension to AGC.

In order to maintain the control of frequency in a much smooth manner, robust secondary controllers are required, which can guarantee negligible area control error. The importance of secondary controllers is highlighted in many literatures.¹⁵⁻²¹ Nanda *et al.* in Ref. 4 used the classical integral (I) controller for solving the AGC problem. The authors have discussed about the two-degree-of-freedom proportional integral derivative (2DOF-PID) controller in Ref. 6, and Saikia *et al.*¹⁵ explored another intelligent controller, fuzzy integral double derivative for a multi-area power system. Debbarma *et al.* implemented the concept of fractional order (FO) controllers in AGC in Refs. 16 and 17. Dash *et al.* demonstrated cascaded controllers (CCs) such as the proportional Integral-proportional derivative (PI-PD) in Ref. 18. Although works related to both the FO controller and the CC are analyzed separately, however, the performance evaluation of the combination of both the concepts still remains unexplored. Thus, the application of the fractional order cascade controller (FOCC) in AGC is needed to be evaluated.

It is necessary to set the controllers' gains at the optimum values, and this is attained using suitable optimisation techniques. Several optimisation techniques like genetic algorithm,⁶ particle swarm optimization (PSO),⁸ biogeography based optimisation,⁹ flower pollination algorithm,¹⁷ firefly algorithm (FA),¹⁸ and cuckoo search (CS)¹⁹ are preferred over the classical technique⁴ as it is a trial and error method and requires an ample amount of time to provide the sub-optimal results. A more recent technique proposed by Mirjalili²⁰ named as the Sine Cosine Algorithm (SCA) is also available whose performance is yet to be evaluated in AGC. The major sense of motivation behind choosing SCA for optimization of the parameters in the present work is that SCA, being a population-based algorithm, is able to avoid local optima and is highly suitable for solving real challenging problems as it explores the search space and exploits the global optimum more reliably.²⁰ Moreover, SCA has the advantage of having only three tuning parameters, namely, number of search agents, number of iterations, and a constant a , which makes it a faster approach. SCA also has least chances of getting trapped in the local optima.

The power outputs of the renewable energy sources are unpredictable and fluctuating in nature which may lead to unreliable and poor power supply.²¹ Hence, to mitigate this, energy storage (ES) elements like battery ES (BES),^{21,22} flywheel ES (FES),^{21,22} capacitive ES (CES),²³ superconducting magnetic ES (SMES),²⁴ ultra-capacitors (UCs),^{21,22} or redox flow batteries (RFBs)^{23,24} can be integrated so that power is uninterruptedly supplied to the load, and simultaneously, minimum system cost can be achieved. Pan and Das²¹ and Das *et al.*²² employed BES, FES, and UC in autonomous hybrid systems having wind, solar, and diesel generators. Saha and Saikia²³ integrated CES and RFB in three area wind-hydro-thermal systems for conventional AGC. SMES was studied by Padhan *et al.*²⁴ for two area thermal systems. If there is surplus power available from the renewable sources over the demanded load, the ES devices store them for a short period of time and later release them to the grid when the

demand load is higher than the generation. They also decrease fluctuations in the grid frequency, thereby improving the power quality. It is seen that the authors of the above literatures^{21–25} have applied various ES devices in diverse fields. However, no literature has made any comparative analysis among all the existing ES devices mentioned above in the presence of the FO proportional-integral–FO proportional-integral-derivative (FOPI-FOPID) as a secondary controller in a system comprising GTPP and having more than two control areas. Hence, further study is necessary in this aspect.

Considering the above cases, the main objectives that can be formulated for the present work are

- (a) To integrate GTPP in an area of a three unequal area system having hydro, wind, and SPV in area1, area2, and area3, respectively, along with the thermal unit, considering appropriate generation rate constraints (GRCs).
- (b) Optimization of different controller gains like I, proportional integral (PI), PID, cascade combination of fractional order (FO) PI and FO proportional integral derivative controller (FOPI-FOPID), and other parameters using the SCA technique and comparison of dynamic responses to find the best.
- (c) To study the effect of GTPP when introduced to the system having hydro, wind, and SPV in area1, area2, and area3, respectively, along with the thermal unit using the best controller identified at (b).
- (d) Comparison of the performance of various ES devices in the system (a) in the presence of the SCA optimised best controller found in (b) to identify the most suitable one.

II. SYSTEM INVESTIGATED

The system considered is a three unequal area multi-source system having a capacity ratio of 1:4:8. GTPP is incorporated only in area1 of the system which comprises hydrothermal units in area1, thermal and wind units in area2, and thermal and SPV plants in area3. GRC is 3%/min for thermal systems, and raising and lowering values for the hydro system are 270%/min and 360%/min, respectively. The nominal parameters for thermal, hydro, wind, and SPV units are taken from Refs. 4, 12, 15, and 26, respectively, and given in Table I. Several classical controllers such as I, PI, and PID are considered for secondary controllers. The controller gains and governor and turbine time constants of GTPP are optimized using the SCA technique. The system dynamics are obtained considering 1% step load perturbation in area1. The transfer function (T.F) model of the system is shown in Fig. 1. The cost function used in this optimization is integral squared error (ISE) and is given by (1). MATLAB software is used for the Simulink Model and execution of programmable codes

$$J_{ISE} = \int_0^T [(\Delta f_i)^2 + (\Delta P_{tiej-k})^2] dt, \quad (1)$$

where i = area number (1,2,3), j = area number (1,2), and $k = 2$ (for $k \neq j$), 3.

III. SYSTEM COMPONENTS, CONTROLLER, AND OPTIMIZATION TECHNIQUE

A. Geothermal power plant (GTPP)

Geothermal power is a potential and reliable source of energy in terms of electricity generation. The Geothermal Energy Association estimated that the global geothermal market is at about 13.3 GW of operating capacity as of January 2016, spread across 24 countries.²⁷ Based on current data, the global geothermal industry is expected to reach about 18.4 GW by 2021. The largest installed capacities are in United States having 3567 MW, followed by Philippines with 1868 MW of capacity online until January 2017 as per the data available with ThinkGeoEnergy. As the behaviour of GTPP is similar to that of a conventional non-reheat

TABLE I. Nominal parameters of the system.

System	Nominal parameters
System model	$f = 60 \text{ Hz}$; loading = 50%, $K_{pi} = 120 \text{ Hz/p.u. MW}$; $T_{pi} = 20 \text{ s}$; $T_{ij} = 0.086 \text{ p.u. MW/rad}$; $H_i = 5 \text{ s}$; $D_i = 8.33 \times 10^{-3} \text{ p.u. MW/Hz}$; $B_i = \beta_i = 0.425 \text{ p.u. MW/Hz}$; $R_i = 2.4 \text{ p.u. Hz/MW}$
Thermal system	$T_{gi} = 0.08 \text{ s}$; $T_{ii} = 0.3 \text{ s}$; $T_{ri} = 10 \text{ s}$; $K_{ri} = 0.5$
Hydro system	$K_d = 4$; $K_p = 1$; $K_i = 5$
Wind system	$T_{P2} = 0.041 \text{ s}$; $K_{P2} = 1.25$; $T_{P1} = 0.6 \text{ s}$; $K_{P3} = 1.4$; $K_{PC} = 0.8$
Solar photovoltaic system	$T_{SPV} = 1.8 \text{ s}$
Battery energy storage (BES)	$K_{BES} = -0.003$; $T_{BES} = 0.1 \text{ s}$
Flywheel energy storage (FES)	$K_{FES} = -0.01$; $T_{FES} = 0.1 \text{ s}$
Capacitive energy storage (CES)	$K_{CES} = 0.3$; $T_{CES} = 0.0352 \text{ s}$
Superconducting magnetic energy storage (SMES)	$K_{SMES} = 0.12$; $T_{SMES} = 0.03 \text{ s}$
Ultra-capacitors (UC)	$K_{UC} = -0.7$; $T_{UC} = 0.9 \text{ s}$
Redox flow battery (RFB)	$K_{RFB} = 0.67$; $T_{RFB} = 0 \text{ s}$

thermal plant with the only difference of the absence of the boiler for reheating the steam, its mathematical modelling is analogous to the latter.²⁶ A block diagram of the GTPP is presented in Fig. 1(b).²⁸ The modelling of governor and turbine units is referred from Refs. 1 and 29. Thus, modelling the governor and turbine leads to a first order transfer function (T.F), dependent only on the time constant of main inlet volumes and steam chest, and is given by $G_G(s) = \frac{1}{g s + 1}$ and $G_T(s) = \frac{1}{t s + 1}$, respectively. The exact values for the time constant of the governor and steam turbine are obtained by optimization using SCA, and their limits are taken from Ref. 1.

When steam enters a turbine, it expands, reducing its pressure and density significantly. No turbine is ideal; hence, the losses are needed to be considered. This is done with the turbine isentropic efficiency (η_s), which denotes the ratio between actual work produced and the maximum theoretical work, and is given by

$$\text{Isentropic efficiency, } \eta_s = \frac{\dot{W}}{\dot{W}_s} = \frac{\dot{m}_{in}(h_{in} - h_{out})}{\dot{m}_{in}(h_{in} - h_{s,out})}, \quad (2)$$

where \dot{W} denotes the work done per unit time, \dot{W}_s is turbine's power output, \dot{m}_{in} is the mass flow rate (kg/s) in the input, h_{in} and h_{out} are the specific enthalpy, and $h_{s,out}$ is the specific enthalpy at the outlet.^{30,31}

B. Fractional order cascade controller (FOPI-FOPID)

The concept of cascade control along with fractional calculus is incorporated in the modelled system which resulted in FOCC. The concepts of FO controller deal with differential equations using fractional calculus, and the commonly used definition for fractional integral and derivative is given by the Riemann–Liouville (R–L) definition¹⁶ in Ref. 17. Using Laplace transformation, while assuming zero initial conditions, the systems which are described by differential equations having fractional derivatives generate transfer functions with fractional order of s . This work uses the *CRONE* (Commande robuste d'ordre non-entier) approximation, proposed by Oustaloup out of several approximations like Carlson, Matsuda, High-frequency continued fraction approximation, and Low-frequency continued fraction approximation.¹⁷ *CRONE* uses a recursive distribution of N poles and N zeros, leading to a transfer function within the prespecified frequency range (ω_l, ω_h). For simulation, $\omega_l = 0.01 \text{ rad/s}$, $\omega_h = 50 \text{ rad/s}$, and $N = 3$ are considered.¹⁶

$PI^{\lambda}D^{\mu}$ is the simplest form of the FO controller whose T.F is given by (3). λ and μ are the FO operators and can be any real numbers¹⁷

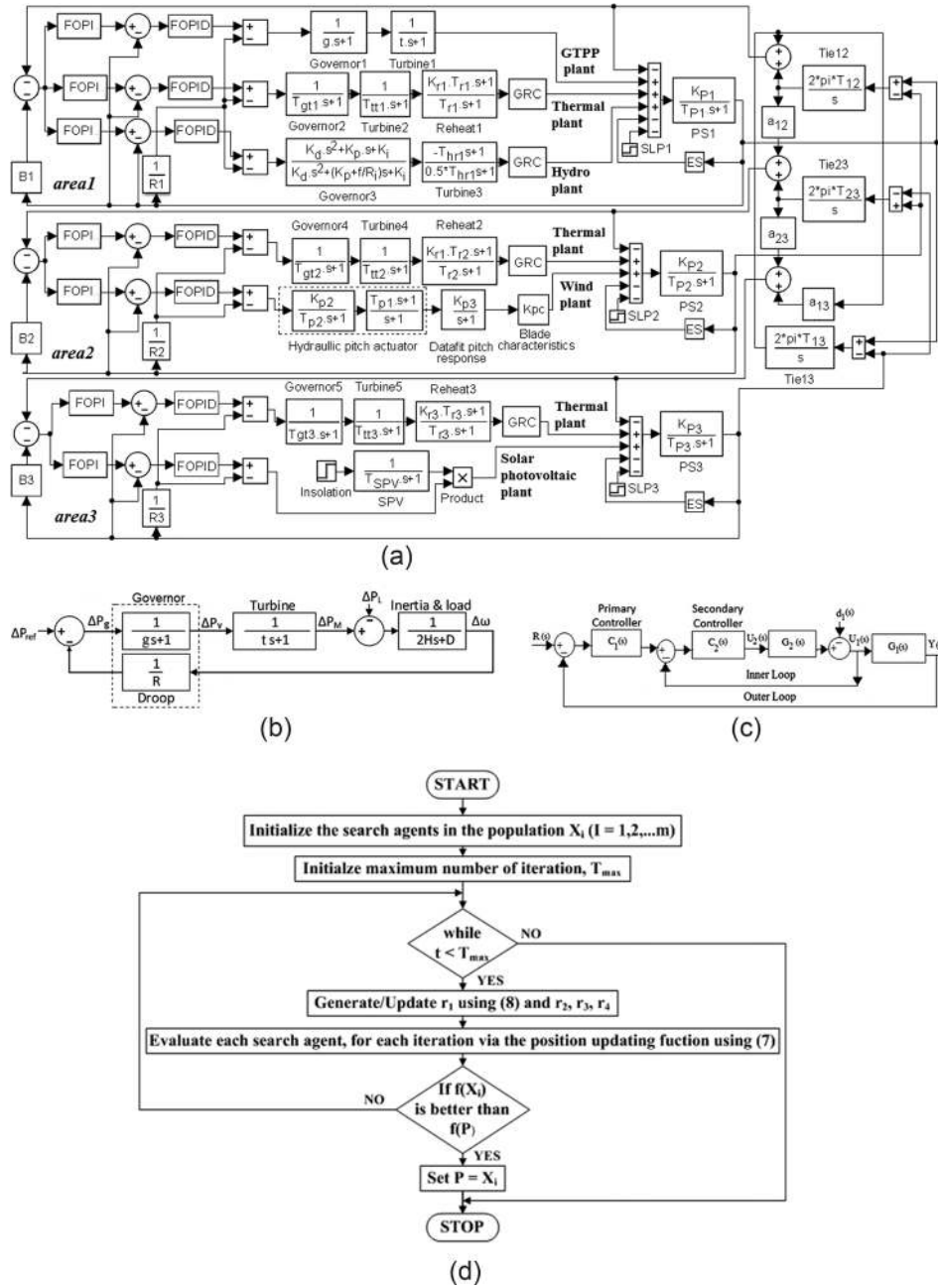


FIG. 1. System component description. (a) Transfer function model of the three unequal area FOPI-FOPID controller based hydrothermal-wind thermal-SPV thermal system along with GTPP only in area1, (b) geothermal power plant model, (c) block diagram for the cascade controller, and (d) sine cosine algorithm flowchart.

$$G_c(s) = K_p + \frac{K_i}{s} + K_d s^u. \tag{3}$$

The addition of filters diminishes the effect of high frequency noise that arises due to continuous switching in the load end and is not desirable. FO controllers are themselves suitable for controlling the dynamics; hence, the concept of cascading the FO controllers can further enhance the performance.

Controlling of two sequential processes leads to the concept of cascade control. Cascade control can improve control system performance over single-loop control. The simplest cascade

control system incorporates two control loops [Fig. 1(c)].¹⁸ The output of the first process, which is the inner loop, supplies the second process or outer loop in sequence. Cascade control is used for rejecting the disturbance in a comparatively faster manner so that it is unable to propagate to other parts of the plant. The outer or primary loop acts as the master and is responsible for controlling the quality of final output. The outer process is termed as $G_1(s)$, and the whole process is subjected to load disturbance $d_1(s)$ producing an output $Y(s)$.

The outer process output must be controlled to attain a given reference signal $R(s)$.¹⁹ The inner loop is the secondary loop that acts as the slave. It attenuates the effect of any disturbance due to the internal process or supply on the outer process.

In this paper, the designed system includes FO controllers that are combined to form a cascaded system. The FOPI controller is cascaded with FOPID, where FOPI forms the outer controller $C_1(s)$ and FOPID the inner one $C_2(s)$ which are given by the following equations:

$$C_1(s) = K_p + \frac{K_i}{s^\lambda}, \quad (4)$$

$$C_2(s) = K_p + \frac{K_i}{s^\lambda} + K_d s^\mu \left(\frac{N}{s^\mu + N} \right). \quad (5)$$

Hence, the closed loop T.F which analyzes the overall performance of the cascaded system is

$$Y(s) = \left[\frac{G_1(s)G_2(s)C_1(s)C_2(s)}{1 + G_2(s)C_2(s) + G_1(s)G_2(s)C_1(s)C_2(s)} \right] R(s) + \left(\frac{G_1(s)}{1 + G_2(s)C_2(s) + G_1(s)G_2(s)C_1(s)C_2(s)} \right) d_1(s). \quad (6)$$

In order to design this FOCC, FOPI–FOPID, for the investigated system, SCA is used.

C. Sine cosine algorithm (SCA)

SCA is a stochastic population-based optimization algorithm developed by Mirjalili,²⁰ which creates multiple initial random solutions, and using a mathematical model based on sine and cosine functions allows them to fluctuate outwards or towards the best solution. SCA maintains a population of m search agents, and each agent is represented by a n -dimension decision variable vector $X_i = (x_{i1}, x_{i2}, \dots, x_{in})$, where X_i is the i -th search agent in the population. Further, the algorithm keeps a track of the best position P of the solution achieved by all search agents at each iteration. The mathematical model used in SCA for any search agent X_i is based on the position updating function which is given by the following equation:³²

$$X_i^{t+1} = \begin{cases} X_i^t + r_1 \times \sin(r_2) \times |r_3 P_i^t - X_i^t| & \text{if } r_4 < 0.5 \\ X_i^t + r_1 \times \sin(r_2) \times |r_3 P_i^t - X_i^t| & \text{if } r_4 \geq 0.5 \end{cases}, \quad (7)$$

where X_i^t is the position of the current solution in the i th dimension at the t th iteration and P_i is the position of the destination point in the i th dimension. r_1 , r_2 , r_3 , and r_4 are the four main parameters, where r_1 depicts the movement direction. r_2 denotes upto which extent the movement should be towards or outwards the destination. r_3 assigns a random weight for the destination in order to emphasize ($r_3 > 1$) or deemphasize ($r_3 < 1$) the effect of destination to define the distance. Finally, r_4 equally switches between the sine and cosine components. The cyclic pattern of sine and cosine functions allows re-positioning of a solution around another solution. To balance exploration and exploitation and eventually converge to the global optimum, the range of sine and cosine in (7) is changed adaptively by the following equation:³³

$$r_1 = a - t \frac{a}{T}, \quad (8)$$

where t is the current iteration, T is the maximum number of iterations, and a is a constant. The tuned values of parameters used in this optimization are $a=2$, number of search agents = 10, and number of iterations = 100. The flowchart for SCA is depicted in Fig. 1(d).

In this paper, SCA is used for simultaneous optimization of controller gains and other parameters. The gains for the secondary controllers I, PI, and PID are optimised one at a time. The gains and the order of integral and derivative gains such as K_{Pi}^* , K_{Ii}^* , and λ_i^* and K_{Pii}^* , K_{Iii}^* , λ_{ii}^* , K_{Dii}^* , and μ_{ii}^* are optimized simultaneously, respectively, and the design problem is formulated with the following constraints. Minimization of the objective function given by (1) is subject to

$$\begin{aligned} K_{Pi}^{\min} \leq K_{Pi} \leq K_{Pi}^{\max}; \quad K_{Ii}^{\min} \leq K_{Ii} \leq K_{Ii}^{\max}; \quad K_{Pii}^{\min} \leq K_{Pii} \leq K_{Pii}^{\max}; \\ K_{Iii}^{\min} \leq K_{Iii} \leq K_{Iii}^{\max}; \quad K_{Dii}^{\min} \leq K_{Dii} \leq K_{Dii}^{\max}; \quad \lambda_i^{\min} \leq \lambda_i \leq \lambda_i^{\max}; \\ \lambda_{ii}^{\min} \leq \lambda_{ii} \leq \lambda_{ii}^{\max}; \quad \mu_{ii}^{\min} \leq \mu_{ii} \leq \mu_{ii}^{\max}; \end{aligned} \quad (9)$$

where K_{Pi}^{\min} , K_{Ii}^{\min} , K_{Pii}^{\min} , K_{Iii}^{\min} , K_{Dii}^{\min} are minimum values, K_{Pi}^{\max} , K_{Ii}^{\max} , K_{Pii}^{\max} , K_{Iii}^{\max} , K_{Dii}^{\max} maximum values of the controller gains, and λ_i^{\min} , λ_{ii}^{\min} , μ_{ii}^{\min} , λ_i^{\max} , λ_{ii}^{\max} , μ_{ii}^{\max} are minimum and maximum values of the order of integral and derivative gains. The minimum and maximum bounds for all the parameters are chosen as 0 and 1, respectively. A detailed picture of the algorithm is however discussed in Ref. 20.

IV. MODELLING OF ENERGY STORAGE DEVICES

A. Battery energy storage (BES)

The BES has been an effective ES technology to store a large amount of renewable energy due to its large energy density and fast access time. BES can supply a large amount of power to the system within a short time or a large amount of energy for a longer period. It stores electric energy in the battery in the form of dc, and hence, it consists of a battery bank and a power converter that interfaces the battery bank to the autonomous utility grid. The time constant of BES is limited to several seconds as it takes time to charge energy to the battery cells. Its T.F is expressed as follows:^{21,22}

$$G_{BES} = \frac{K_{BES}}{T_{BESS} + 1}. \quad (10)$$

B. Flywheel energy storage (FES)

FES is more suitable than BES for repetitively absorbing and releasing electric energy for a short period of time. FES operates by storing energy mechanically in a rotating flywheel. It stores energy in the form of kinetic energy and has the ability to store surplus power during off-peak hours and quickly release energy during peak periods. FES is most suited for short time turbulent power pulsation produced by renewables. Reliability, fast response, long-life span, and being cheaper are some of its assets, while less stored energy per volume, higher losses, and increased volume and mass are the major loop holes. The T.F is given by the following equation:^{21,22}

$$G_{FES} = \frac{K_{FES}}{T_{FESS} + 1}. \quad (11)$$

C. Capacitive energy storage (CES)

CES has the unique characteristic to respond rapidly to power changes and so is more preferable compared to other ES like FES. CES comprises storage capacitors and a power conversion system (PCS). The PCS consists of an inverter/rectifier, and it serves the purpose of connecting the capacitors to the ac grid. Under normal operation of the grid, the capacitor can be charged from the utility grid to a set value of voltage. This set value is less than the full charge. Reversing switch arrangement is used with the help of a gate turn-off thyristor in order to change the direction of current through the capacitor during charging and discharging operation.

This is done as the direction of current through the bridge converters cannot be changed. CES can also act as a spinning reserve to ensure stability during disturbances. The T.F is expressed by the following equation:²³

$$G_{CES} = \frac{K_{CES}}{T_{CES}s + 1}. \quad (12)$$

D. Superconducting magnetic energy storage (SMES)

SMES utilizes the magnetic field of a coil to store electrical power from the grid. The magnetic field of coil is made of superconducting wire with a negligible loss of energy. SMES can store a huge amount of energy. Hence, almost instantaneously, it is able to compensate the high levels of power discharged by the power system, thus avoiding rapid loss of power. SMES consists of an inductor-converter unit, a dc superconducting inductor, an AC/DC converter, and a step down transformer. As all parts of SMES are static, its stability is much more superior to other ES devices. The charged superconducting coil conducts current and is immersed in liquid helium to maintain a very low temperature. When there is a sudden rise in load demand, stored energy is rapidly released to the grid as ac power via a PCS. The coil charges back to its initial value of current as control mechanisms start working to set the power system to the new equilibrium condition. Its T.F is given by the following equation:²⁴

$$G_{SMES} = \frac{K_{SMES}}{T_{SMES}s + 1}. \quad (13)$$

E. Ultra-capacitors (UCs)

UC, also known as a supercapacitor, is another emerging device for ES. It stores charge in a double layer formed on a large surface area of micro-porous material such as activated carbon. Hence, it is also called the double layer capacitor. UC carries with itself a large number of advantages of having a high power density, good charge/discharge efficiency, and much higher life cycle than batteries. In addition, their manufacturing cost is decreasing rapidly. UC in combination with batteries appears to be a power source of high power capability and longer run time. Neglecting all the non-linearities, its T.F is given by the following equation:^{21,22}

$$G_{UC} = \frac{K_{UC}}{T_{UC}s + 1}. \quad (14)$$

F. Redox flow battery (RFB)

RFB, which is developed since the 1970s, has evolved as the most prominent rechargeable electrochemical ES device due to its stationary ES technologies. RFB converts and stores electrical energy in chemical form to generate electricity in a controlled manner by a reduction–oxidation (redox) reaction whenever required. The RFB reactor consists of the electrolyte of sulfuric acid (H_2SO_4) solution with vanadium pentoxide (V_2O_5). There are two compartments which are segregated by a proton exchange membrane. Each compartment is linked to a reservoir tank and a pump so that very large volumes of the electrolytes can be circulated through the cell. The battery charges and delivers energy to the system instantly during the peak or sudden load demands. A dual converter performs both the rectifier and inverter action. When there is a delay in the governor response or other mechanisms, RFB due to its lag timing provides fast storing action, thus eliminating the oscillations in a disturbed system. The lag timing has an advantage of diminishing the hunting. In order to maintain energy, fresh electrolytes are continuously pumped into the battery. Thus, the control signal is directly fed to the RFB units. RFB is easy to operate at normal temperature, is capable of ensuring a very quick response, has very small losses under operating conditions, and ensures a long service life and a reduced impact on the environment. These characteristics are more than enough to consider RFB as a superior

TABLE II. Optimal gains for the I controller and GTPP parameters.

Controllers	Optimal gains				
I	$K_{igl}^* = 0.1318$	$K_{iil}^* = 0.1733$	$K_{ihl}^* = 0.1898$	$K_{iiz}^* = 0.844$	$K_{iw2}^* = 0.1614$
	$K_{is3}^* = 0.2166$	$K_{is3}^* = 0.9$	$g^* = 0.05$	$t^* = 0.1$	

option over the other ES. Such features allow for wide ranges of operational powers and discharge times, thus making RFB ideal for electricity generation from renewable sources. Its T.F represented by the following equation:^{23,25}

$$G_{RFB} = \frac{K_{RFB}}{T_{RFB}S + 1}. \quad (15)$$

The value of gains and time constant for each ES is given in Table I.

V. RESULTS AND ANALYSIS

A. Comparison of performance of I, PI, PID, and FOPI-FOPID for the system with GTPP

The three unequal area multi-source system incorporating GTPP is investigated with I, PI, PID, and FOPI-FOPID controllers one at a time. The I controller gains and the parameters for GTPP are simultaneously optimized at first using SCA. The optimum values are presented in Table II. The governor and the turbine time constants for GTPP are obtained in this case, and the same constant values are considered for the remaining cases. Thus, taking the GTPP parameters from Table II, the system is provided with PI, PID, and FOPI-FOPID controllers, one at a time, and in each case controller, gains are simultaneously optimized using SCA (Table III).

TABLE III. Optimal gains for PI, PID, and FOPI-FOPID controllers for the system with GTPP.

Controllers	Optimal gains				
PI	$K_{pg1}^* = 0.01$	$K_{igl}^* = 0.01$	$K_{pt1}^* = 0.01$	$K_{iil}^* = 0.9999$	$K_{ph1}^* = 0.01$
	$K_{ih1}^* = 0.0158$	$K_{pt2}^* = 0.0212$	$K_{it2}^* = 0.0168$	$K_{pw1}^* = 0.0498$	$K_{iw2}^* = 0.0232$
	$K_{pt3}^* = 0.01$	$K_{is3}^* = 0.9999$	$K_{ps3}^* = 0.9999$	$K_{is3}^* = 0.9999$	
PID	$K_{pg1}^* = 0.9$	$K_{igl}^* = 0.9$	$K_{dg1}^* = 0.9$	$K_{ng1}^* = 100$	$K_{pt1}^* = 0.2355$
	$K_{iil}^* = 0.1$	$K_{dit}^* = 0.2235$	$K_{ni1}^* = 48.4191$	$K_{ph1}^* = 0.1212$	$K_{ih1}^* = 0.7926$
	$K_{dh1}^* = 0.01$	$K_{nh1}^* = 83.1556$	$K_{pt2}^* = 0.7740$	$K_{it2}^* = 0.2512$	$K_{dt2}^* = 0.1$
	$K_{nt2}^* = 33.308$	$K_{pw2}^* = 0.9$	$K_{iw2}^* = 0.1$	$K_{dw2}^* = 0.1199$	$K_{nw2}^* = 24.268$
	$K_{pt3}^* = 0.4140$	$K_{is3}^* = 0.3817$	$K_{dt3}^* = 0.8120$	$K_{nt3}^* = 79.423$	$K_{ps3}^* = 0.1$
	$K_{is3}^* = 0.2355$	$K_{ds3}^* = 0.2644$	$K_{ns3}^* = 100$		
FOPI-FOPID cascade	$K_{pg1}^* = 0.4919$	$K_{igl}^* = 0.8556$	$\lambda_{g1}^* = 0.7605$	$K_{pg11}^* = 0.831$	$K_{ig11}^* = 0.8762$
	$\lambda_{g11}^* = 0.7644$	$K_{dg11}^* = 0.1748$	$\mu_{g11}^* = 0.1089$	$K_{pt1}^* = 0.1973$	$K_{iil}^* = 0.1$
	$\lambda_{t1}^* = 0.0163$	$K_{pt11}^* = 0.3331$	$K_{iil1}^* = 0.1031$	$\lambda_{i11}^* = 0.2078$	$K_{dt11}^* = 0.5127$
	$\mu_{i11}^* = 0.3313$	$K_{ph1}^* = 0.8155$	$K_{ih1}^* = 0.1214$	$\lambda_{h1}^* = 0.1957$	$K_{ph11}^* = 0.1680$
	$K_{ih11}^* = 0.1002$	$\lambda_{h11}^* = 0.8612$	$K_{dh11}^* = 0.0136$	$\mu_{h11}^* = 0.1010$	$K_{pt2}^* = 0.6633$
	$K_{it2}^* = 0.1815$	$\lambda_{t2}^* = 0.4940$	$K_{pt22}^* = 0.1$	$K_{it22}^* = 0.2552$	$\lambda_{t22}^* = 0.3164$
	$K_{dt22}^* = 0.1$	$\mu_{t22}^* = 0.1$	$K_{pw2}^* = 0.1297$	$K_{iw2}^* = 0.4138$	$\lambda_{w2}^* = 0.1010$
	$K_{pw22}^* = 0.2331$	$K_{iw22}^* = 0.1796$	$\lambda_{w22}^* = 0.3073$	$K_{dw22}^* = 0.1051$	$\mu_{w22}^* = 0.9$
	$K_{pt3}^* = 0.1$	$K_{it3}^* = 0.4494$	$\lambda_{t3}^* = 0.1$	$K_{pt33}^* = 0.1051$	$K_{it33}^* = 0.1241$
	$\lambda_{t33}^* = 0.1$	$K_{dt33}^* = 0.2292$	$\mu_{t33}^* = 0.2700$	$K_{ps3}^* = 0.1240$	$K_{is3}^* = 0.1$
	$\lambda_{s3}^* = 0.6538$	$K_{ps3}^* = 0.2356$	$K_{is33}^* = 0.6508$	$\lambda_{s33}^* = 0.3513$	$K_{ds33}^* = 0.3062$
	$\mu_{s33}^* = 0.4016$				

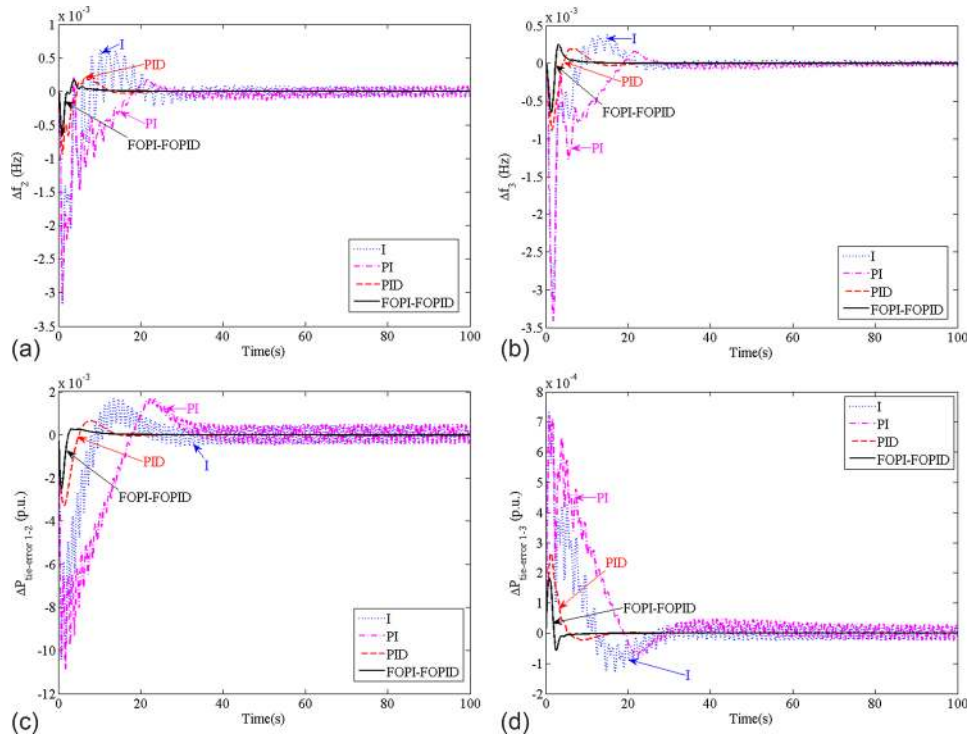


FIG. 2. Comparison of dynamic responses of I, PI, PID, and FOPI-FOPD controllers for the hydrothermal-wind thermal-SPV thermal system incorporating GTPP. (a) Frequency deviation in area2 vs. time, (b) frequency deviation in area3 vs. time, (c) deviation in tie-line power error in the line connecting area1 and area2 vs. time, and (d) deviation in tie-line power error in the line connecting area1 and area3 vs. time.

The dynamic responses for each controller are obtained and compared in Fig. 2. Observation of the settling time and peak deviations in Fig. 2 firmly speak out the predominance of the FOPI-FOPID controller over I, PI, and PID controllers from the points of view of settling time and magnitude of oscillations.

B. Comparison of algorithms

The system considered in Sec. V A is taken here to compare the convergence characteristics of various algorithms. The controller gains and other parameters are optimized using FA, CS, and PSO techniques separately (the optimum values are not shown). The convergence characteristics of each are obtained and compared with those of SCA and shown in Fig. 3. Critical observation of the convergence characteristics evidently reveals that SCA converges comparatively faster in comparison to others.

C. Effect of GTPP

The effect of GTPP on the system dynamics is analysed by introducing it to the multi-source system having hydro, wind, and SPV in area1, area2, and area3, respectively, along with the thermal unit, maintaining the same system capacity. Considering FOPI-FOPID controllers as secondary controllers in all the areas, the controller and other parameters are optimized simultaneously using SCA for the system without GTPP (Table IV). The obtained dynamic responses are then compared with those corresponding to optimum values of the system having GTPP (Table III). From careful observation of this comparison, [Figs. 4(a)–4(d)], it is clearly evident that inclusion of GTPP improves the system dynamic responses from the points of view of settling time, peak overshoot, and magnitude of oscillations. This is also justified theoretically as the boiler is not required for reheating the steam in GTPPs. The absence of the boiler,

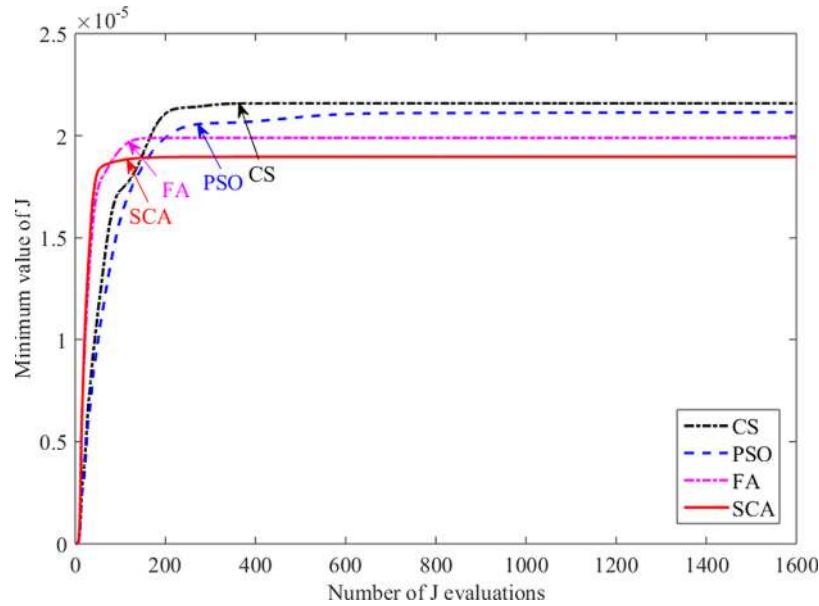


FIG. 3. Convergence curve.

re-heater, makes the system responses better, which leads to the simple first order transfer function. The time constants of the governor and the turbine are quite small, which is another important reason for GTPP giving a better response.²⁸ Thus, for the remaining studies, the GTPP incorporated system is considered.

D. Performance comparison of several ES devices in the system incorporating GTPP

In this section, the considered system with GTPP is provided with several ES devices such as BES, FES, CES, SMES, UC, and RFB separately one at a time in all the areas. The FOPI-FOPID controller is used as a secondary controller in each of the cases, and the controller gains and other parameters are optimized using SCA. The optimum values of the GTPP incorporated system for each of the ES obtained are shown in Table V. Using these optimum values, dynamic responses are procured for each ES device and all of them are simultaneously compared with those of the system having GTPP but without ES (fifth row in Table III) in Fig. 5. From the performance comparison of the dynamic responses of all the ES devices, it is clearly evident that the responses corresponding to each ES have enhanced remarkably compared to

TABLE IV. Optimal gains for FOPI-FOPID controllers for the system without GTPP.

Controllers	Optimal gains				
FOPI-FOPID cascade	$K_{pt1}^* = 0.9$	$K_{it1}^* = 0.7774$	$\lambda_{t1}^* = 0.9999$	$K_{pt11}^* = 0.1$	$K_{it11}^* = 0.1$
	$\lambda_{i11}^* = 0.1470$	$K_{dt11}^* = 0.8996$	$\mu_{t11}^* = 0.1$	$K_{phi1}^* = 0.1837$	$K_{ih1}^* = 0.4873$
	$\lambda_{h1}^* = 0.1$	$K_{ph11}^* = 0.1231$	$K_{ih11}^* = 0.1001$	$\lambda_{h11}^* = 0.1560$	$K_{dh11}^* = 0.0122$
	$\mu_{h11}^* = 0.0285$	$K_{pt2}^* = 0.2380$	$K_{it2}^* = 0.9309$	$\lambda_{t2}^* = 0.01$	$K_{pt22}^* = 0.9$
	$K_{it22}^* = 0.1$	$\lambda_{t22}^* = 0.9$	$K_{dt22}^* = 0.8921$	$\mu_{t22}^* = 0.1$	$K_{pw2}^* = 0.9$
	$K_{iw2}^* = 0.1$	$\lambda_{w2}^* = 0.1$	$K_{pw22}^* = 0.2512$	$K_{iw22}^* = 0.1$	$\lambda_{w22}^* = 0.1$
	$K_{dw22}^* = 0.1$	$\mu_{w22}^* = 0.1$	$K_{pt3}^* = 0.5594$	$K_{it3}^* = 0.9564$	$\lambda_{t3}^* = 0.9999$
	$K_{pt33}^* = 0.9$	$K_{it33}^* = 0.1226$	$\lambda_{t33}^* = 0.1093$	$K_{dt33}^* = 0.1068$	$\mu_{t33}^* = 0.9$
	$K_{ps3}^* = 0.5372$	$K_{is3}^* = 0.1028$	$\lambda_{s3}^* = 0.1$	$K_{ps3}^* = 0.9$	$K_{is33}^* = 0.1$
	$\lambda_{s33}^* = 0.6918$	$K_{ds33}^* = 0.2985$	$\mu_{s33}^* = 0.1$		

TABLE V. FOPI-FOPID optimal gains for different ES devices connected in the hydrothermal-wind thermal-SPV thermal system incorporating GTPP.

Energy storage	FOPI-FOPID cascade controller optimal gains				
BES	$K_{pg1}^* = 0.8521$	$K_{ig1}^* = 0.8990$	$\lambda_{g1}^* = 0.6523$	$K_{pg11}^* = 0.6297$	$K_{ig11}^* = 0.8814$
	$\lambda_{g11}^* = 0.8604$	$K_{dg11}^* = 0.8850$	$\mu_{g11}^* = 0.4968$	$K_{pt1}^* = 0.1312$	$K_{it1}^* = 0.7341$
	$\lambda_{t1}^* = 0.2443$	$K_{pt11}^* = 0.2910$	$K_{it11}^* = 0.4860$	$\lambda_{t11}^* = 0.3229$	$K_{dt11}^* = 0.6715$
	$\mu_{t11}^* = 0.7694$	$K_{ph1}^* = 0.2841$	$K_{ih1}^* = 0.3153$	$\lambda_{h1}^* = 0.7185$	$K_{ph11}^* = 0.1000$
	$K_{ih11}^* = 0.6921$	$\lambda_{h11}^* = 0.8200$	$K_{dh11}^* = 0.0107$	$\mu_{h11}^* = 0.1661$	$K_{pt2}^* = 0.3496$
	$K_{it2}^* = 0.8180$	$\lambda_{t2}^* = 0.2377$	$K_{pt22}^* = 0.4071$	$K_{it22}^* = 0.6618$	$\lambda_{t22}^* = 0.7813$
	$K_{dt22}^* = 0.5576$	$\mu_{t22}^* = 0.4639$	$K_{pw2}^* = 0.6734$	$K_{iw2}^* = 0.2589$	$\lambda_{w2}^* = 0.3390$
	$K_{pw22}^* = 0.6678$	$K_{iw22}^* = 0.4891$	$\lambda_{w22}^* = 0.8200$	$K_{dw22}^* = 0.2011$	$\mu_{w22}^* = 0.8785$
	$K_{pt3}^* = 0.4888$	$K_{it3}^* = 0.3722$	$\lambda_{t3}^* = 0.2866$	$K_{pt33}^* = 0.4398$	$K_{it33}^* = 0.8819$
	$\lambda_{t33}^* = 0.5137$	$K_{dt33}^* = 0.3044$	$\mu_{t33}^* = 0.6536$	$K_{ps3}^* = 0.6909$	$K_{is3}^* = 0.2472$
	$\lambda_{s3}^* = 0.1462$	$K_{ps3}^* = 0.2783$	$K_{is33}^* = 0.8551$	$\lambda_{s33}^* = 0.2179$	$K_{ds33}^* = 0.7612$
	$\mu_{s33}^* = 0.1518$				
FES	$K_{pg1}^* = 0.8971$	$K_{ig1}^* = 0.8980$	$\lambda_{g1}^* = 0.5314$	$K_{pg11}^* = 0.8963$	$K_{ig11}^* = 0.9000$
	$\lambda_{g11}^* = 0.9681$	$K_{dg11}^* = 0.8995$	$\mu_{g11}^* = 0.2467$	$K_{pt1}^* = 0.1427$	$K_{it1}^* = 0.7569$
	$\lambda_{t1}^* = 0.7405$	$K_{pt11}^* = 0.7381$	$K_{it11}^* = 0.5236$	$\lambda_{t11}^* = 0.7167$	$K_{dt11}^* = 0.8942$
	$\mu_{t11}^* = 0.6447$	$K_{ph1}^* = 0.4071$	$K_{ih1}^* = 0.5875$	$\lambda_{h1}^* = 0.2195$	$K_{ph11}^* = 0.1003$
	$K_{ih11}^* = 0.6837$	$\lambda_{h11}^* = 0.8979$	$K_{dh11}^* = 0.1007$	$\mu_{h11}^* = 0.1060$	$K_{pt2}^* = 0.8641$
	$K_{it2}^* = 0.4026$	$\lambda_{t2}^* = 0.6648$	$K_{pt22}^* = 0.5383$	$K_{it22}^* = 0.4484$	$\lambda_{t22}^* = 0.3783$
	$K_{dt22}^* = 0.6417$	$\mu_{t22}^* = 0.6513$	$K_{pw2}^* = 0.2559$	$K_{iw2}^* = 0.6003$	$\lambda_{w2}^* = 0.5256$
	$K_{pw22}^* = 0.8489$	$K_{iw22}^* = 0.1179$	$\lambda_{w22}^* = 0.5009$	$K_{dw22}^* = 0.6621$	$\mu_{w22}^* = 0.2665$
	$K_{pt3}^* = 0.7771$	$K_{it3}^* = 0.1771$	$\lambda_{t3}^* = 0.3220$	$K_{pt33}^* = 0.2259$	$K_{it33}^* = 0.1753$
	$\lambda_{t33}^* = 0.2840$	$K_{dt33}^* = 0.3026$	$\mu_{t33}^* = 0.7738$	$K_{ps3}^* = 0.4237$	$K_{is3}^* = 0.6804$
	$\lambda_{s3}^* = 0.5978$	$K_{ps3}^* = 0.7352$	$K_{is33}^* = 0.5777$	$\lambda_{s33}^* = 0.7609$	$K_{ds33}^* = 0.7217$
	$\mu_{s33}^* = 0.6813$				
CES	$K_{pg1}^* = 0.8798$	$K_{ig1}^* = 0.9000$	$\lambda_{g1}^* = 0.8209$	$K_{pg11}^* = 0.5780$	$K_{ig11}^* = 0.8808$
	$\lambda_{g11}^* = 0.7595$	$K_{dg11}^* = 0.7428$	$\mu_{g11}^* = 0.4450$	$K_{pt1}^* = 0.7148$	$K_{it1}^* = 0.5318$
	$\lambda_{t1}^* = 0.7737$	$K_{pt11}^* = 0.1730$	$K_{it11}^* = 0.3936$	$\lambda_{t11}^* = 0.1802$	$K_{dt11}^* = 0.8200$
	$\mu_{t11}^* = 0.8581$	$K_{ph1}^* = 0.4512$	$K_{ih1}^* = 0.2717$	$\lambda_{h1}^* = 0.7230$	$K_{ph11}^* = 0.1665$
	$K_{ih11}^* = 0.2602$	$\lambda_{h11}^* = 0.8628$	$K_{dh11}^* = 0.0100$	$\mu_{h11}^* = 0.1023$	$K_{pt2}^* = 0.6451$
	$K_{it2}^* = 0.5050$	$\lambda_{t2}^* = 0.3547$	$K_{pt22}^* = 0.5431$	$K_{it22}^* = 0.4043$	$\lambda_{t22}^* = 0.1287$
	$K_{dt22}^* = 0.4438$	$\mu_{t22}^* = 0.3832$	$K_{pw2}^* = 0.3252$	$K_{iw2}^* = 0.1398$	$\lambda_{w2}^* = 0.2889$
	$K_{pw22}^* = 0.2507$	$K_{iw22}^* = 0.9000$	$\lambda_{w22}^* = 0.2382$	$K_{dw22}^* = 0.4668$	$\mu_{w22}^* = 0.9000$
	$K_{pt3}^* = 0.8200$	$K_{it3}^* = 0.4770$	$\lambda_{t3}^* = 0.2725$	$K_{pt33}^* = 0.1000$	$K_{it33}^* = 0.3857$
	$\lambda_{t33}^* = 0.7279$	$K_{dt33}^* = 0.5666$	$\mu_{t33}^* = 0.8584$	$K_{ps3}^* = 0.2019$	$K_{is3}^* = 0.1935$
	$\lambda_{s3}^* = 0.1966$	$K_{ps3}^* = 0.6312$	$K_{is33}^* = 0.2722$	$\lambda_{s33}^* = 0.6986$	$K_{ds33}^* = 0.7082$
	$\mu_{s33}^* = 0.2344$				
SMES	$K_{pg1}^* = 0.9000$	$K_{ig1}^* = 0.9000$	$\lambda_{g1}^* = 0.6519$	$K_{pg11}^* = 0.8336$	$K_{ig11}^* = 0.7526$
	$\lambda_{g11}^* = 0.9478$	$K_{dg11}^* = 0.6519$	$\mu_{g11}^* = 0.7368$	$K_{pt1}^* = 0.5506$	$K_{it1}^* = 0.5461$
	$\lambda_{t1}^* = 0.4962$	$K_{pt11}^* = 0.5954$	$K_{it11}^* = 0.7466$	$\lambda_{t11}^* = 0.6138$	$K_{dt11}^* = 0.5291$
	$\mu_{t11}^* = 0.2008$	$K_{ph1}^* = 0.6323$	$K_{ih1}^* = 0.9000$	$\lambda_{h1}^* = 0.1872$	$K_{ph11}^* = 0.1648$
	$K_{ih11}^* = 0.2600$	$\lambda_{h11}^* = 0.5805$	$K_{dh11}^* = 0.1029$	$\mu_{h11}^* = 0.1000$	$K_{pt2}^* = 0.2663$
	$K_{it2}^* = 0.2140$	$\lambda_{t2}^* = 0.7659$	$K_{pt22}^* = 0.3588$	$K_{it22}^* = 0.8275$	$\lambda_{t22}^* = 0.3129$
	$K_{dt22}^* = 0.4501$	$\mu_{t22}^* = 0.4483$	$K_{pw2}^* = 0.5043$	$K_{iw2}^* = 0.2277$	$\lambda_{w2}^* = 0.8735$
	$K_{pw22}^* = 0.4004$	$K_{iw22}^* = 0.5375$	$\lambda_{w22}^* = 0.7209$	$K_{dw22}^* = 0.6584$	$\mu_{w22}^* = 0.2564$
	$K_{pt3}^* = 0.8064$	$K_{it3}^* = 0.7765$	$\lambda_{t3}^* = 0.2196$	$K_{pt33}^* = 0.2916$	$K_{it33}^* = 0.7559$
	$\lambda_{t33}^* = 0.8065$	$K_{dt33}^* = 0.4172$	$\mu_{t33}^* = 0.4909$	$K_{ps3}^* = 0.7908$	$K_{is3}^* = 0.2905$

TABLE V. (Continued.)

Energy storage	FOPI-FOPID cascade controller optimal gains				
	$\lambda_{s3}^* = 0.1754$ $\mu_{s33}^* = 0.2456$	$K_{ps3}^* = 0.3321$	$K_{is33}^* = 0.5526$	$\lambda_{s33}^* = 0.4110$	$K_{ds33}^* = 0.6779$
UC	$K_{pg1}^* = 0.8921$ $\lambda_{g11}^* = 0.9973$ $\lambda_{i1}^* = 0.2534$ $\mu_{i11}^* = 0.0172$ $K_{ih11}^* = 0.3806$ $K_{i2}^* = 0.5887$ $K_{dt22}^* = 0.9602$ $K_{pw22}^* = 0.1588$ $K_{pt3}^* = 0.8609$ $\lambda_{t33}^* = 0.5149$ $\lambda_{s3}^* = 0.5376$ $\mu_{s33}^* = 0.0512$	$K_{ig1}^* = 0.8984$ $K_{dg11}^* = 0.9894$ $K_{pt11}^* = 0.5393$ $K_{ph1}^* = 0.3836$ $\lambda_{h11}^* = 0.8053$ $\lambda_{t2}^* = 0.8125$ $\mu_{t22}^* = 0.0183$ $K_{iw22}^* = 0.6576$ $K_{it3}^* = 0.4603$ $K_{ps3}^* = 0.5990$	$\lambda_{g1}^* = 0.3969$ $\mu_{g11}^* = 0.0254$ $K_{it11}^* = 0.8155$ $K_{ih1}^* = 0.4655$ $K_{dih11}^* = 0.0105$ $K_{pt22}^* = 0.3169$ $K_{pw2}^* = 0.7487$ $\lambda_{w22}^* = 0.6950$ $\lambda_{t3}^* = 0.3616$ $\mu_{t33}^* = 0.0234$ $K_{is33}^* = 0.2489$	$K_{pg11}^* = 0.8038$ $K_{pt1}^* = 0.2158$ $\lambda_{t11}^* = 0.6530$ $\lambda_{h1}^* = 0.7320$ $\mu_{h11}^* = 0.0115$ $K_{it22}^* = 0.3505$ $K_{iw2}^* = 0.4662$ $K_{dw22}^* = 0.9784$ $K_{pt33}^* = 0.6567$ $K_{ps3}^* = 0.5788$ $\lambda_{s33}^* = 0.7791$	$K_{ig11}^* = 0.9000$ $K_{it1}^* = 0.6220$ $K_{dt11}^* = 0.9564$ $K_{ph11}^* = 0.1416$ $K_{pt2}^* = 0.7557$ $\lambda_{t22}^* = 0.2525$ $\lambda_{w2}^* = 0.7760$ $\mu_{w22}^* = 0.0771$ $K_{it33}^* = 0.7394$ $K_{is3}^* = 0.5303$ $K_{ds33}^* = 0.9507$
RFB	$K_{pg1}^* = 0.8965$ $\lambda_{g11}^* = 0.9673$ $\lambda_{i1}^* = 0.5951$ $\mu_{i11}^* = 0.6566$ $K_{ih11}^* = 0.1607$ $K_{i2}^* = 0.8031$ $K_{dt22}^* = 0.7331$ $K_{pw22}^* = 0.2076$ $K_{pt3}^* = 0.5831$ $\lambda_{t33}^* = 0.4503$ $\lambda_{s3}^* = 0.3795$ $\mu_{s33}^* = 0.3811$	$K_{ig1}^* = 0.8945$ $K_{dg11}^* = 0.8783$ $K_{pt11}^* = 0.1830$ $K_{ph1}^* = 0.5594$ $\lambda_{h11}^* = 0.8627$ $\lambda_{t2}^* = 0.6314$ $\mu_{t22}^* = 0.3027$ $K_{iw22}^* = 0.3295$ $K_{it3}^* = 0.3203$ $K_{ps3}^* = 0.3207$	$\lambda_{g1}^* = 0.5196$ $\mu_{g11}^* = 0.1000$ $K_{it11}^* = 0.3571$ $K_{ih1}^* = 0.5949$ $K_{dih11}^* = 0.1001$ $K_{pt22}^* = 0.8462$ $K_{pw2}^* = 0.6660$ $\lambda_{w22}^* = 0.3874$ $\lambda_{t3}^* = 0.7338$ $\mu_{t33}^* = 0.7870$ $K_{is33}^* = 0.6502$	$K_{pg11}^* = 0.9000$ $K_{pt1}^* = 0.4429$ $\lambda_{t11}^* = 0.7608$ $\lambda_{h1}^* = 0.4389$ $\mu_{h11}^* = 0.1153$ $K_{it22}^* = 0.9839$ $K_{iw2}^* = 0.6856$ $K_{dw22}^* = 0.2624$ $K_{pt33}^* = 0.7136$ $K_{ps3}^* = 0.5827$ $\lambda_{s33}^* = 0.4413$	$K_{ig11}^* = 0.9999$ $K_{it1}^* = 0.1702$ $K_{dt11}^* = 0.7479$ $K_{ph11}^* = 0.1824$ $K_{pt2}^* = 0.2407$ $\lambda_{t22}^* = 0.7485$ $\lambda_{w2}^* = 0.3659$ $\mu_{w22}^* = 0.4374$ $K_{it33}^* = 0.5008$ $K_{is3}^* = 0.4957$ $K_{ds33}^* = 0.4908$

that without ES. Hence, if there is an energy storage device in the system, then some of the extra power will be drawn from it as a result of which less kinetic energy is utilized to mitigate the small load demand. Thus, integration of the energy storage devices improves the responses. Further, RFB responses are far more superior compared to other ES from the point of view of magnitude of oscillations, settling time, and peak deviations.

VI. CONCLUSION

An attempt of analysing the performance of several ES devices in the presence of a new FOCC, FOPI-FOPID, is initiated for the first time in the AGC environment. GTPP is proposed to be introduced to the three area system having hydro, wind, and SPV in area1, area2, and area3, respectively, along with the thermal system. The SCA technique is successfully used for simultaneous optimization of different controller and system parameters. The system dynamic performance using the newly proposed FOPI-FOPID controller is found to be much better than that using the classical controllers. It is also concluded that system dynamics are improved to a great extent when GTPP is incorporated to the system. Further, inclusion of several ES devices to the system having GTPP was tested one at a time. Analyses suggest the inclusion of ES; furthermore, RFB can be declared as the most preferable ES among others. Thus, the authors recommend its use along with the other sources to solve the AGC problem.

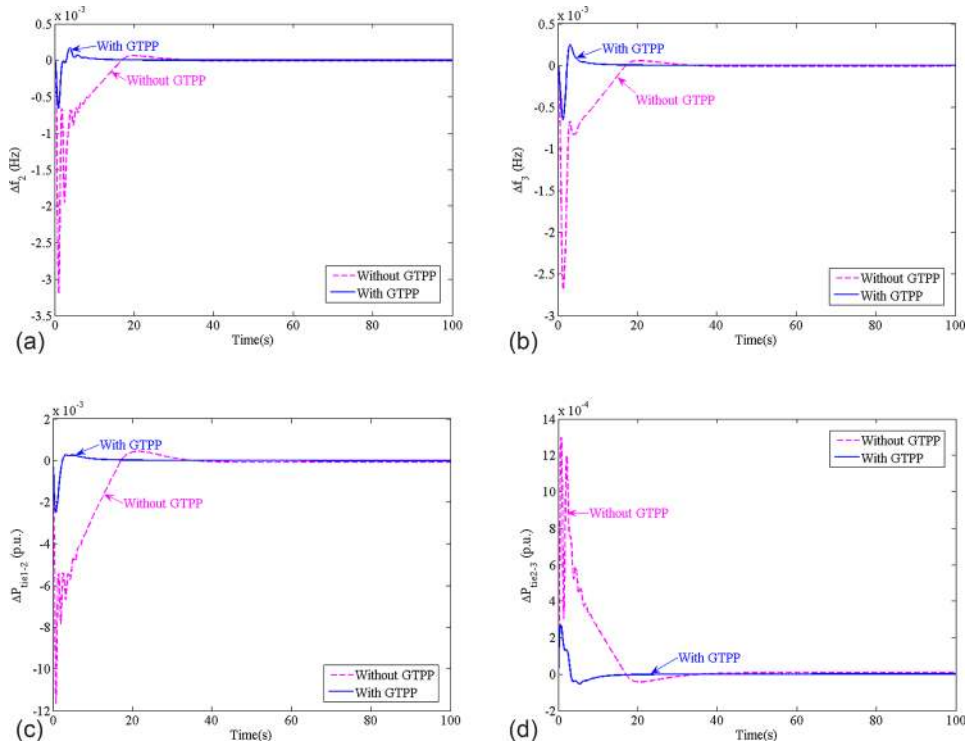


FIG. 4. Comparison of dynamic responses of the hydrothermal-wind thermal-SPV thermal system with and without GTPP. (a) Frequency deviation in area2 vs. time, (b) frequency deviation in area3 vs. time, (c) deviation in tie-line power error in the line connecting area1 and area2 vs. time, and (d) deviation in tie-line power error in the line connecting area2 and area3 vs. time.

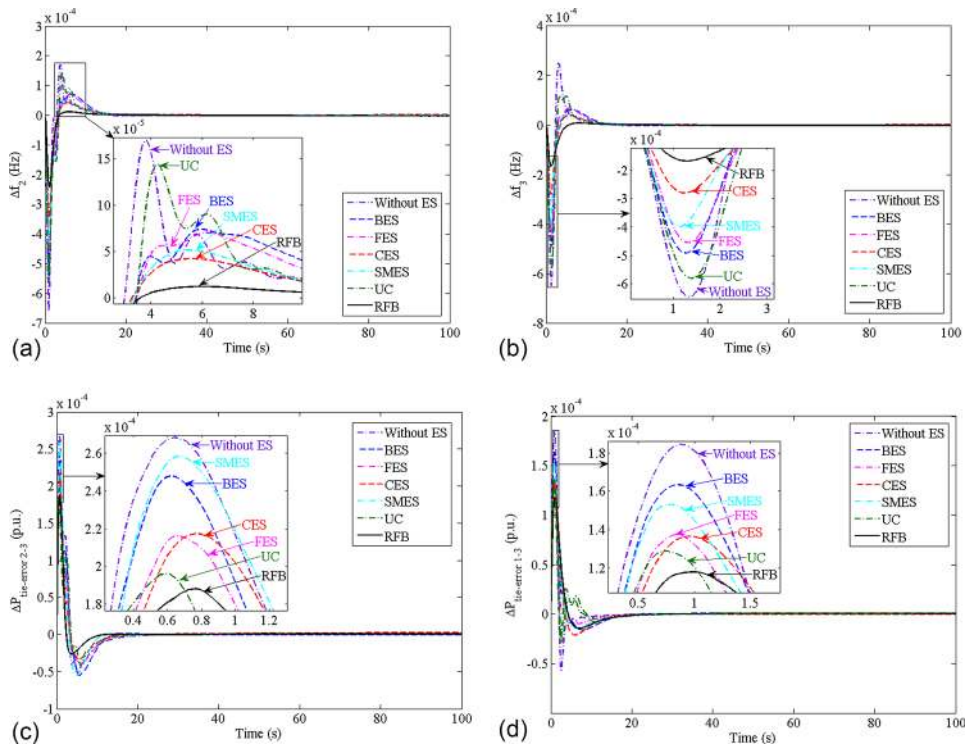


FIG. 5. Comparison of dynamic responses of several ES devices for the GTPP incorporated system. (a) Frequency deviation in area2 vs. time, (b) frequency deviation in area3 vs. time, (c) deviation in tie-line power error in the line connecting area2 and area3 vs. time, and (d) deviation in tie-line power error in the line connecting area1 and area3 vs. time.

- ¹O. I. Elgerd, *Electric Energy Systems Theory: An Introduction*, 2nd ed. (Tata McGraw-Hill, New Delhi, 1983).
- ²K. P. Ibraheem and D. P. Kothari, "Recent philosophies of automatic generation control strategies in power systems," *IEEE Trans. Power Syst.* **20**(1), 346–357 (2005).
- ³J. Nanda and B. L. Kaul, "Automatic generation control of an interconnected power system," *Electr. Eng., Proc. Inst.* **125**(5), 385–390 (1978).
- ⁴J. Nanda, S. Mishra, and L. C. Saikia, "Maiden application of bacterial foraging-based optimization technique in multi area automatic generation control," *IEEE Trans. Power Syst.* **24**(2), 602–609 (2009).
- ⁵L. C. Saikia, J. Nanda, and S. Mishra, "Performance comparison of several classical controllers in AGC for multi-area interconnected thermal system," *Int. J. Electr. Power Energy Syst.* **33**(3), 394–401 (2011).
- ⁶R. K. Sahu *et al.*, "Teaching learning based optimization algorithm for automatic generation control of power system using 2-DOF PID controller," *Int. J. Electr. Power Energy Syst.* **77**, 287–301 (2016).
- ⁷H. Bevrani, A. Ghosh, and G. Ledwich, "Renewable energy sources and frequency regulation: Survey and new perspectives," *IET Renewable Power Gener.* **4**(5), 438–457 (2010).
- ⁸Y. Sharma and L. C. Saikia, "Automatic generation control of a multi-area ST—Thermal power system using Grey Wolf Optimizer algorithm based classical controllers," *Electr. Power Energy Syst.* **73**, 853–862 (2015).
- ⁹A. Rahman, L. Saikia, and N. Sinha, "AGC of dish-Stirling solar thermal integrated thermal system with biogeography based optimised three degree of freedom PID controller," *IET Renewable Power Gener.* **10**(8), 1161–1170 (2016).
- ¹⁰H. Asano, K. Yajima, and Y. Kaya, "Influence of photovoltaic power generation on required capacity for load frequency control," *IEEE Trans. Energy Convers.* **11**(1), 188–193 (1996).
- ¹¹D.-J. Lee and L. Wang, "Small-signal stability analysis of an autonomous hybrid renewable energy power generation/energy storage system part I: Time-domain simulations," *IEEE Trans. Energy Convers.* **23**(1), 311–320 (2008).
- ¹²I. Pan and S. Das, "Fractional order AGC for distributed energy resources using robust optimization," *IEEE Trans. Smart Grid* **7**(5), 2175–2186 (2016).
- ¹³J. Buchta, "Green power from conventional steam power plant combined with geothermal well," in *IEEE International Conference on Industrial Technology, ICIT* (IEEE, 2009).
- ¹⁴A. Setel *et al.*, "Use of geothermal energy to produce electricity at average temperatures," in *13th International Conference on Engineering of Modern Electric Systems (EMES)* (IEEE, 2015).
- ¹⁵L. C. Saikia, N. Sinha, and J. Nanda, "Maiden application of bacterial foraging based fuzzy IDD controller in AGC of a multi-area hydrothermal system," *Int. J. Electr. Power Energy Syst.* **45**(1), 98–106 (2013).
- ¹⁶S. Debbarma and A. Dutta, "Utilizing electric vehicles for LFC in restructured power systems using fractional order controller," *IEEE Trans. Smart Grid* **8**(6), 2554–2564 (2017).
- ¹⁷S. Debbarma, L. C. Saikia, N. Sinha, B. Kar, and A. Datta, "Fractional order two degree of freedom control for AGC of an interconnected multi-source power system," in *2016 IEEE International Conference on Industrial Technology (ICIT)*, Taipei (2016), pp. 505–510.
- ¹⁸P. Dash, L. C. Saikia, and N. Sinha, "Flower pollination algorithm optimized PI-PD cascade controller in automatic generation control of a multi-area power system," *Int. J. Electr. Power Energy Syst.* **82**, 19–28 (2016).
- ¹⁹P. Dash, L. C. Saikia, and N. Sinha, "Automatic generation control of multi area thermal system using Bat algorithm optimized PD-PID cascade controller," *Int. J. Electr. Power Energy Syst.* **68**, 364–372 (2015).
- ²⁰S. Mirjalili, "SCA: A sine cosine algorithm for solving optimization problems," *Knowl.-Based Syst.* **96**, 120–133 (2016).
- ²¹I. Pan and S. Das, "Fractional order fuzzy control of hybrid power system with renewable generation using chaotic PSO," *ISA Trans.* **62**, 19–29 (2016).
- ²²D. C. Das, A. K. Roy, and N. Sinha, "GA based frequency controller for solar thermal–diesel–wind hybrid energy generation/energy storage system," *Int. J. Electr. Power Energy Syst.* **43**(1), 262–279 (2012).
- ²³D. Saha and L. C. Saikia, "Performance of FACTS and energy storage devices in a multi area wind-hydro-thermal system employed with SFS optimized I-PDF controller," *J. Renewable Sustainable Energy* **9**(2), 024103 (2017).
- ²⁴S. Padhan, R. K. Sahu, and S. Panda, "Automatic generation control with thyristor controlled series compensator including superconducting magnetic energy storage units," *Ain Shams Eng. J.* **5**(3), 759–774 (2014).
- ²⁵A. Yogendra and N. Kumar, "Optimal AGC with redox flow batteries in multi-area restructured power systems," *Eng. Sci. Technol., Int. J.* **19**(3), 1145–1159 (2016).
- ²⁶D. Das, S. K. Aditya, and D. P. Kothari, "Dynamics of diesel and wind turbine generators on an isolated power system," *Int. J. Electr. Power Energy Syst.* **21**, 183–189 (1999).
- ²⁷M. S. Hossain *et al.*, "Role of smart grid in renewable energy: An overview," *Renewable Sustainable Energy Rev.* **60**, 1168–1184 (2016).
- ²⁸B. Heimisson, "Improved frequency control strategies for geothermal power plants," M.S. thesis (Chalmers University of Technology, Sweden, 2014).
- ²⁹P. Kundur, *Power System Stability and Control* (Mc Graw Hill, 1993).
- ³⁰Ö. N. Yıldırım, "Modeling, simulation and optimization of flashed-steam geothermal power plants from the point of view of no condensable gas removal systems," Ph.D. thesis (İzmir Institute of Technology, Turkey, 2010).
- ³¹Á. J. Ólafsson, "Verification of design models for geothermal power plants," M.S. thesis (University of Iceland, 2014).
- ³²M. Urfi and S. Prashar, "A comprehensive literature review on load frequency control strategies," *Int. J. Sci., Eng. Technol. Res. (IJSETR)* **5**(11), 3220–3229 (2016).
- ³³M. Urfi and S. Prashar, "Load frequency control of two area thermal system using sine-cosine algorithm," *Int. J. Sci., Eng. Technol. Res. (IJSETR)* **6**(4), 497–503 (2017).